Polymer 227 (2021) 123854

Contents lists available at ScienceDirect

Polymer

journal homepage: www.elsevier.com/locate/polymer

Correlating crystalline structure with charge mobility in conjugated statistical copolymers for field-effect transistors

Dongqi Huang, Juan Peng *

State Key Laboratory of Molecular Engineering of Polymers, Department of Macromolecular Science, Fudan University, Shanghai, 200438, China

ARTICLE INFO

Keywords:
Conjugated statistical copolymers
Crystallization
Field-effect mobilities

ABSTRACT

Since thiophene and selenophene have comparable molecular structures and possess individual remarkable optoelectronic characteristics, crystals comprising both units may exhibit improved charge mobility than their respective homopolymers due to the synergy. This, however, has yet to be largely utilized in statistical copolymers. In this study, a series of poly(3-butylthiophene)-*stat*-poly(3-hexylselenophene) (P3BT-*stat*-P3HS) statistical copolymers with variable molar ratios of thiophene to selenophene were synthesized and investigated in respect of thermal, crystalline, and charge transport properties. All three P3BT-*stat*-P3HS copolymers were found to well crystallize in an edge-on configuration in spite of their random arrangement of thiophene and selenophene units along the main backbones. Consequently, high-performance organic field-effect transistors (OFETs) were achieved in as-cast P3BT-*stat*-P3HS crystals, surpassing those of P3BT, P3HS and P3BT/P3HS blend. After 150 °C thermal annealing, the charge mobilities of these statistical copolymers were further slightly enhanced due to the improved crystallinities as well as more ordered crystalline structures. This work shows the improved field-effect mobilities in conjugated polymer-based statistical copolymers due to the synergy of thiophene and selenophene units. Such P3BT-*stat*-P3HS crystals may be used in diverse printable flexible electronics owing to their excellent charge mobilities and annealing-free properties.

1. Introduction

Organic field-effect transistors (OFETs) based on conjugated polymers have attracted much interest due to their light weight, solution processability, and excellent charge transport properties [1,2]. As the most important parameter in OFET devices, the charge carrier mobility (μ) is subject to their chemical structure, molecular stacking, crystalline structure and morphology within the active layer on multiple length scales [3]. On one hand, from the molecular design perspective, a large number of novel conjugated polymers have been synthesized with well-defined chemical structure and good charge mobilities due to the great advances in synthetic techniques [4–7]. On the other hand, tailoring their condensed state structure including the molecular packing, crystalline structure, etc. is receiving increasingly attention since the charge transport is a complicated multi-scale process [8–11]. In the latter context, a set of extrinsic parameters such as solvent [12], aging [13], the addition of additives [14], thermal annealing [15], solvent vapor annealing [16], and applying electric field [17] have been utilized to tune the crystalline structures of conjugated polymers efficiently.

Up to now, most of OFETs comprising conjugated polymers are based on single constituent possessing its own intrinsic properties. The aggregation of two or more conjugated constituents into crystalline structures may confer them with novel properties and diverse functionalities, which is promising for OFETs [18]. Among a number of conjugated polymers, poly(3-alkylthiophene)s (P3ATs), have been widely researched as the model systems. P3ATs have a hair-rod configuration which can preferentially pack into an edge-on orientation where the alkyl sidechains (*a*-axis) is perpendicular to the substrate and both the π-π stacking (*b*-axis) and the main backbone (*c*-axis) are parallel to the substrate [19]. Compared to P3ATs, poly(3-alkylselenophene)s (P3ASs), the close analogues of P3ATs, are much less studied due to difficulty in synthesis and relatively poor solubility [20]. The physical and chemical properties of P3ASs and P3ATs are relatively close. Nonetheless, P3ASs have a more planar backbone and a narrower bandgap compared to P3ATs [20]. These characteristics are beneficial for the improvement of light absorption and charge carrier mobility. However, P3AS-based OFETs do not outperform P3ATs in terms of charge carrier mobility due to the poor solubility resulting from

* Corresponding author.
E-mail address: juanpeng@fudan.edu.cn (J. Peng).

https://doi.org/10.1016/j.polymer.2021.123854
Received 2 April 2021; Received in revised form 8 May 2021; Accepted 10 May 2021
Available online 18 May 2021

the stronger Se–Se interaction and the increased π-π stacking distance arising from the larger Se atoms. Since P3ATs and P3ASs carry respective excellent optoelectronic properties, it is conceivable that the copolymers composed of both of them may have better performance than their respective components.

In general, there are two ways to combine two different conjugated polymers, i.e., simply blending them without covalent bonds and copolymerization with covalent bonds. In the latter, the copolymerization can be divided into block copolymerization, alternating copolymerization, graft copolymerization, and random copolymerization according to the arrangement order of structural units [21–25]. For example, several all-conjugated block copolymers comprising P3AT or P3AS blocks have been reported, among which poly(3-butylthiophene)-*block*-poly(3-hexylselenophene) (P3BT-*b*-P3HS) [18] and poly (2,5-dihexyloxy-p-phenylene)-*block* -poly(3-(2- ethylhexyl)thiophene) (PPP-*b*-P3EHT) [25] are found to have cocrystalline structures. Statistical copolymers containing thiophene or selenophene building block may possess properties distinct from the block copolymers and their blends, however, are relatively less explored [26–30].

Herein, a set of poly(3-butylthiophene)-*stat*-poly(3-hexylselenophene) (P3BT-*stat*-P3HS) statistical copolymers were rationally designed and synthesized with varying molar ratios of thiophene to selenophene via Grignard metathesis (GRIM) polymerization. Butylthiophene and hexylselenophene units were chosen based on the consideration that the butylthiophene units can pack more closely which favor interchain charge transport, and the hexylselenophene units have a higher planarity which facilitate intrachain charge transport. Their optical, crystalline and thermal properties have been elucidated through a suite of characterization techniques including ultraviolet–visible (UV–vis) spectroscopy, cyclic voltammetry (CV), differential scanning calorimetry (DSC) and grazing-incidence X-ray diffraction (GIXRD), etc. By controlling the composition ratio of thiophene to selenophene, their optical bandgaps could be precisely tuned. Quite interestingly, the presence of crystals adopting an edge-on orientation were recognized in P3BT-*stat*-P3HS thin films, despite the random sequence of thiophene and selenophene units along the main backbone, beneficial to high charge mobility. Importantly, these P3BT-*stat*-P3HS crystals exhibited excellent field-effect mobilities in the absence of further thermal or solvent treatments, surpassing those of P3BT, P3HS, and P3BT/P3HS blend. The average charge mobility of *stat*-BT70HS30 reaches up to $\mathbf{5.9 \times 10^{-2}}$ $cm^2 V^{-1} s^{-1}$, demonstrating excellent compatibility and synergy of thiophene and selenophene units connected covalently within the mainchains. In stark contrast, the charge mobility of P3BT/P3HS blend was lower than P3BT-*stat*-P3HS crystals and its parent P3BT and P3HS homopolymers due to its separated P3BT and P3HS crystalline domains with quantities of grain boundaries as well as the absence of adequate bridging chains between crystalline domains. After 150 °C thermal annealing, the crystallinities of P3BT-*stat*-P3HS were enhanced, leading to slightly higher charge mobilities compared with those in as-cast state. As such, the P3BT-*stat*-P3HS copolymers possess a number of desirable characteristics including tunable bandgap, crystalline nature and relatively high mobilities, and thus may find diverse potential applications in optoelectronic devices.

2. Experimental section

Materials. 2-bromo-5-iodo-3-butylthiophene and 2,5-dibromo-3-hexylselenophene were synthesized based on the literature [31]. (1, 3-bis(diphenylphosphino)propane)-dichloronickel(II) (Ni(dppp)Cl_2) and isopropylmagnesium chloride (i-PrMgCl, 2.0 M in tetrahydrofuran) were obtained from Sigma-Aldrich. Other solvents were purchased from Sinopharm Chemical Reagent Co., Ltd. (SRC).

Synthesis of Poly(3-butylthiophene)-*stat*-poly(3-hexylselenophene) (P3BT-*stat*-P3HS). P3BT-*stat*-P3HS with varied molar ratios of thiophene to selenophene were synthesized via Grignard metathesis (GRIM) polymerization [32]. Taking the feed molar ratio of 75:75 as an example, the typical procedure for synthesizing P3BT-*stat*-P3HS was as follows. 2-bromo-5-iodo-3-butylthiophene (1.032 g, 3 mmol) and 2,5-dibromo-3-hexylselenophene (1.108 g, 3 mmol) were injected into two respective three-neck flasks pre-dried by heating. Subsequently, THF (50 mL) were loaded into the two flasks to dissolve the monomers. The solutions were cooled to 0 °C, followed by the addition of i-PrMgCl in THF (3 mL, 6 mmol) via a syringe. After 30 min, the two activated monomers were mixed and the copolymerization was initiated via Ni(dppp)Cl_2 (0.0217 g, 0.04 mmol). After stirring the resulting solution at 35 °C for 2 h, the reaction was quenched with HCl (aq) (50 wt %), followed by the precipitation of the product in methanol. The product was filtered and successively Soxhlet extracted with methanol and hexane, and dried under reduced pressure to yield a purple solid. The other two P3BT-*stat*-P3HS with 100:50 and 50:100 feed molar ratios were prepared using the same method.

OFET Device Fabrication. OFETs in a bottom-gate top-contact configuration were crafted on highly n-doped silicon wafers with a layer of 300 nm SiO_2. Acetone, methanol, and isopropanol were used in sequence to clean the wafers. The spotless wafers were then cleaned by plasma (~10 min), followed by modification with n-octadecyltrichlorosilane (ODTS). Thin polymer films were obtained by spin-coating the polymer toluene solution (10 mg/mL) on silicon wafers. The gold with a thickness of 30 nm was evaporated on the polymer films before or after thermal annealing as the source/drain electrodes via a shadow mask. The transistor channel length (L) and width (W) are 30 and 300 μm, respectively. The mobility (μ_{FET}) was derived from the transfer curves based on the following equation [33]:

$$I_{DS} = \frac{W}{2L}\mu_{FET}C_g(V_G - V_T)^2$$

where I_{DS} is the drain current, V_G is the gate voltage, V_T is the threshold voltage, and C_g is the capacitance of the gate dielectric.

2.1. Characterizations

Gel permeation chromatography (GPC) was carried out on an Agilent 1260 system, calibrated with polystyrene standards. ^{1}H NMR spectra were acquired using a DMX500 MHz spectrometer in $CDCl_3$. UV–vis absorption spectra were collected on a PerkinElmer Lambda 750 UV–vis spectrophotometer. Cyclic Voltammetry (CV) curves were recorded on a CHI 660 Electrochemical Analyzer. Grazing-incidence X-ray diffraction (GIXRD) were performed at the BL14B1 beamline (wavelength: 1.24 Å) in Shanghai Synchrotron Radiation Facility (SSRF). TGA measurements were conducted using a Perkin Elmer TGA 4000 under a N_2 environment. Differential scanning calorimetry (DSC) traces were acquired on a TA DSC Q2000 with the heating rate and cooling rate of 10 °C/min and −10 °C/min, respectively. Atomic force microscopy (AFM) were performed at a Bruker Multimode Dimension FastScan in the tapping mode. The OFETs device performance of all samples were characterized utilizing a Keithley 4200-SCS in an argon atmosphere.

3. Results and discussion

A series of P3BT-*stat*-P3HS statistical copolymers with various thiophene to selenophene molar ratios were synthesized through GRIM polymerization (Scheme 1). The 2-bromo-5-iodo-3-butylthiophene monomer and the 2,5-dibromo-3-hexylselenophene monomer were activated by i-PrMgCl, respectively. Subsequently, the two activated monomers were mixed at a certain ratio and the polymerizations were initiated via Ni(dppp)Cl_2 to prepare the target statistical copolymers. These P3BT-*stat*-P3HS have relatively high molecular weights, ranging from 26.0 kDa to 29.9 kDa, a narrow polydispersity index (PDI) of 1.07–1.09, and high regioregularity (RR) of 92%–95% (Figure S1 and Table 1). For comparison, the control samples including P3BT (M_n = 29.4 kDa, PDI = 1.03) and P3HS (M_n = 25.3 kDa, PDI = 1.10)

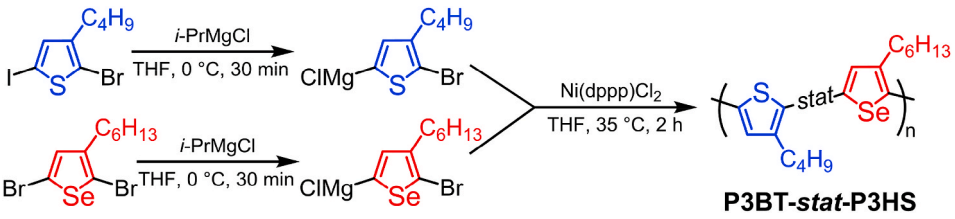

Scheme 1. Synthesis of P3BT-*stat*-P3HS Statistical Copolymers.

Table 1
Summary of compositions and molecular weights of P3BT-*stat*-P3HS statistical copolymers and P3BT and P3HS homopolymers.

polymers	feed molar ratio	n/m^a	M_n (kDa)[b]	PDI	RR (%)[c]
P3BT	–	–	29.4	1.03	93
P3HS	–	–	25.3	1.10	95
stat-BT70HS30	100:50	70:30	26.0	1.09	92
stat-BT56HS44	75:75	56:44	29.9	1.08	94
stat-BT37HS63	50:100	37:63	28.5	1.07	95

[a] Determined by ^{1}H NMR.
[b] Measured by GPC.
[c] Regioregularity determined by ^{1}H NMR.

homopolymers were also synthesized. The percentage of thiophene and selenophene units in the.

Statistical copolymers were determined by ^{1}H NMR (Fig. 1 and Figure S2). The P3BT-*stat*-P3HS statistical copolymers show four aromatic signals, with 6.98 and 6.93 ppm corresponding to the thiophene ring proton, and 7.19 and 7.13 ppm assigned to the selenophene ring proton. Due to the effect of the adjacent heterocycle coupled at 5-position, there are four kinds of dyads (i.e., S–S, S–Se, Se–Se, and Se–S) in a statistical copolymer. This is in contrast to P3BT-*b*-P3HS block copolymer possessing only two types of dyads (i.e., S–S and Se–Se) and thus showing only two peaks at 6.99 and 7.12 ppm, ascribed to the thiophene and selenophene ring proton, respectively [18]. By integrating the corresponding aromatic proton signals, the actual thiophene

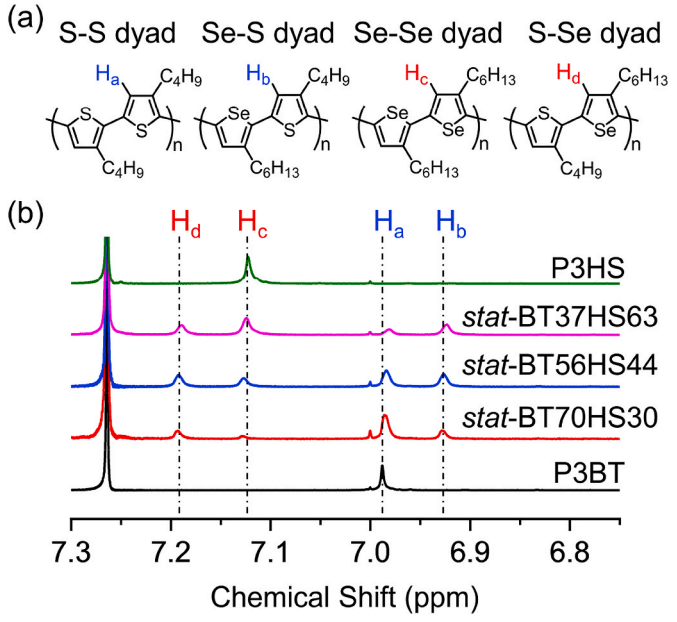

Fig. 1. (a) Four kinds of dyads (i.e., S–S, S–Se, Se–Se, and Se–S) and the corresponding aromatic protons (i.e., H_a, H_b, H_c, and H_d) in P3BT-*stat*-P3HS statistical copolymers. (b) ^{1}H NMR spectra of the selected aromatic region of three P3BT-*stat*-P3HS statistical copolymers and P3BT and P3HS homopolymers in $CDCl_3$.

to selenophene molar ratio within the three P3BT-*stat*-P3HS copolymers were determined to be 70:30, 56:44 and 37:63, which are denoted as *stat*-BT70HS30, *stat*-BT56HS44, and *stat*-BT37HS63, respectively. For each P3BT-*stat*-P3HS statistical copolymer, the fraction of each dyad in the four kinds (S–S, S–Se, Se–Se, Se–S) can be further obtained directly from the integration of the corresponding aromatic signals. Notably, they are all close to expected values based on a perfectly statistical copolymerization model (Figure S3) [28,30]. For three P3BT-*stat*-P3HS, the increased fraction of BT leads to the increased signal of H_a (corresponding to S–S dyad) and the decreased signal of H_c (corresponding to Se–Se dyad). For each statistical copolymer, the intensity of H_b and H_d (corresponding Se–S and S–Se dyad, respectively) is similar without obvious difference. It further confirms the statistical nature of the copolymerization.

To probe the molecular structure and electronic properties of P3BT-*stat*-P3HS, dodecamer comprising the thiophene and selenophene units with the same number was constructed and density functional theory (DFT) calculations were carried out with the B3LYP/6-31G (d, p) as the basis set [34]. Methyl groups were adopted to replace the original alkyl side chains on heterocycle rings to simplify the calculation. Calculations on thiophene dodecamer and selenophene dodecamer were also carried out using the same way for reference. The average dihedral angles of thiophene dodecamer and selenophene dodecamer are 17.4° and 0.02°, respectively, signifying that the backbone of polyselenophene is more planar than that of polythiophene (Fig. 2a and b). The average dihedral angle of statistical dodecamer is 4.2°, lower than that of thiophene dodecamer, indicating that the introduction of selenophene rings to the thiophene backbone improved its planarity markedly (Fig. 2c). Fig. 2d shows that the highest occupied molecular orbital (HOMO) and the lowest unoccupied molecular orbital (LUMO) distribution contours of statistical dodecamer are relatively evenly distributed on thiophene and selenophene units. It implies that both the selenophene and thiophene units have approximately equal effect on determining the bandgap of statistical copolymers. According to the formula: $E_g = 0.68 \times (LUMO_{DFT/B3LYP} - HOMO_{DFT/B3LYP}) + 0.33$ eV [35], the theoretical bandgap (E_g) of thiophene dodecamer, selenophene dodecamer, thiophene-selenophene statistical dodecamer is calculated to be 1.91, 1.69, and 1.76 eV, respectively (Table 2).

In order to gain insight into the optical and electrochemical properties of P3BT-*stat*-P3HS, UV–vis absorption spectroscopy and cyclic voltammetry (CV) were performed, together with P3BT and P3HS homopolymers for comparison. The UV–vis spectra revealed that single peaks were observed in each system in their solution state and the maximum absorption peaks varied almost linearly with the increase of selenophene content (i.e., 455 nm for P3BT, 464 nm for *stat*-BT70HS30, 470 nm for *stat*-BT56HS44, 477 nm for *stat*-BT37HS63, and 490 nm for P3HS) (Fig. 3a). Thus, the optical absorption properties of P3BT-*stat*-P3HS copolymers can be precisely tuned by simply adjusting the composition ratio of thiophene to selenophene. In the thin film state, the maximum absorption peaks of all polymers red-shifted remarkably compared with their absorption in the solution, which are 528, 571, 581, 586, and 590 nm for P3BT, *stat*-BT70HS30, *stat*-BT56HS44, *stat*-BT37HS63, and P3HS, respectively (Fig. 3b). It indicates a more planar backbone conformation and an extended conjugation length of all systems in the thin film state. Two shoulder peaks at around 560 and 610

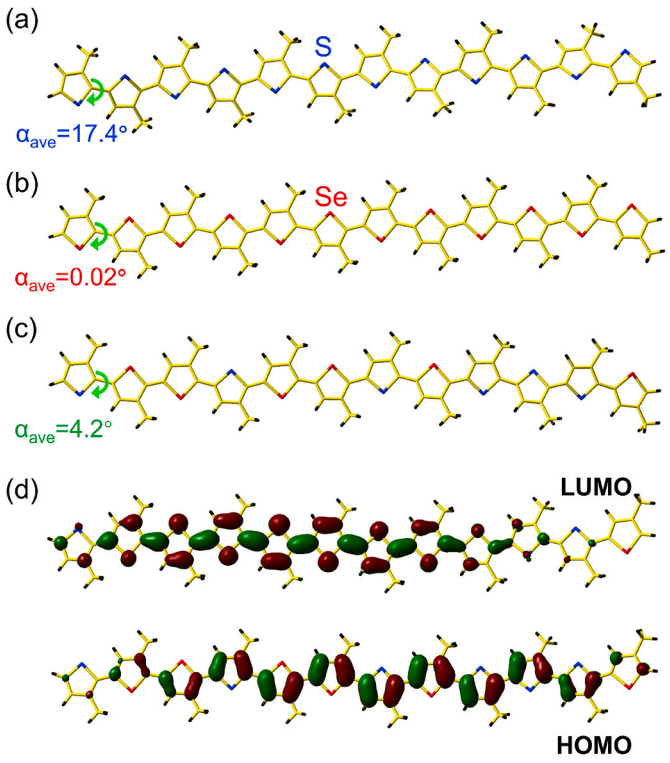

Fig. 2. DFT-simulated molecular structure of (a) thiophene dodecamer, (b) selenophene dodecamer, and (c) P3BT-*stat*-P3HS statistical dodecamer comprising 6 thiophene and 6 selenophene units. (d) DFT calculations on frontier orbital distribution contours for P3BT-*stat*-P3HS statistical dodecamer comprising 6 thiophene and 6 selenophene units.

Table 2
Summary of electrochemical properties of P3BT-*stat*-P3HS statistical copolymers and P3BT and P3HS homopolymers.

Polymers	HOMO (eV)[a]	LUMO (eV)[b]	Experimental Bandgap (eV)[c]	Theoretical Bandgap (eV)[d]
P3BT	−5.03	−3.13	1.90	1.91
P3HS	−5.09	−3.44	1.65	1.69
stat-BT70HS30	−5.04	−3.21	1.83	–
stat-BT56HS44	-5.06	−3.28	1.78	1.76
stat-BT37HS63	−5.08	−3.36	1.72	–

[a] Measured from the onset of oxidation *vs* ferrocene.
[b] Calculated based on the HOMO and optical bandgap.
[c] Determined by the onset of thin film absorption.
[d] Derived from the DFT calculation.

nm were observed for P3BT, indicating the increased ordering of P3BT backbones. P3HS displayed only one single shoulder peak at 690 nm due to the interchain π-π stacking. For three P3BT-*stat*-P3HS copolymers, there was one shoulder peak between 610 and 690 nm for each system, i.e., 621, 638, and 660 nm for *stat*-BT70HS30, *stat*-BT56HS44, and *stat*-BT37HS63, respectively, which could be ascribed to their respective interchain π-π interaction.

The actual E_g of each system can be determined by the onset of their thin film absorption, which is 1.90, 1.83, 1.78, 1.72, and 1.65 eV for P3BT, *stat*-BT70HS30, *stat*-BT56HS44, *stat*-BT37HS63, and P3HS, respectively (Table 2). The E_g of three P3BT-*stat*-P3HS copolymers are between those of P3BT and P3HS homopolymers, which are in good accordance with the theoretical E_g. The actual E_g decreases gradually with the increased selenophene content. It provides an effective way to

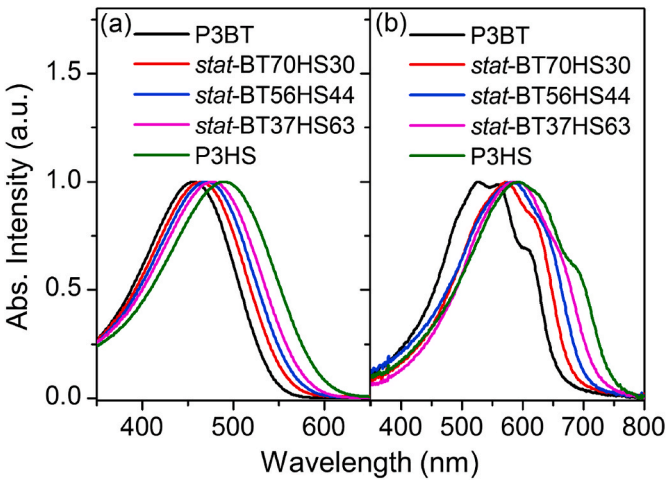

Fig. 3. UV–vis spectra of three P3BT-*stat*-P3HS statistical copolymers and P3BT and P3HS homopolymers in (a) the toluene solutions and (b) in the thin films cast from the toluene solutions.

efficiently control the bandgap of the statistical copolymers by simply tuning the ratio of thiophene to selenophene. Subsequently, the HOMO energy levels of all systems were measured by CV experiments, which are −5.03, −5.04, −5.06, −5.08, and −5.09 eV for P3BT, *stat*-BT70HS30, *stat*-BT56HS44, *stat*-BT37HS63, and P3HS, respectively (Table 2 and Figure S4). On the basis of the HOMO energy levels and the actual E_g, the LUMO energy levels of all systems were then obtained readily, i.e., −3.13 eV for P3BT, −3.21 eV for *stat*-BT70HS30, -3.28 eV for *stat*-BT56HS44, -3.36 eV for *stat*-BT37HS63, and -3.44 eV for P3HS, respectively (Table 2 and Figure S5). It can be seen that with the increased selenophene content, the decrease in bandgap was due largely to the decline in the LUMO energy level. The relatively deep LUMO energy levels can protect the electrons from oxidation, which may endow the P3BT-*stat*-P3HS statistical copolymers with improved photostability [20].

Conjugated polymer thin films comprise both crystalline regions and amorphous regions. In the crystalline regions, the polymer chains possess long conjugation length and pack compactly to form ordered structures, favouring effective interchain and intrachain charge transport [36]. However, the conjugation length of the polymer chains is reduced accompanied with the formation of disordered structures in the amorphous regions, which are detrimental to the charge transport. Thus, charge transport is a complicated multi-scale process, from the molecular structure to the microscopic packing structure and up to the macroscopic film morphology. Hence, 2D-GIXRD measurements were performed so as to investigate the P3BT-*stat*-P3HS crystalline structures, along with the corresponding P3BT and P3HS homopolymers, and P3BT/P3HS blend for comparison. Fig. 4a describes the schematic of the synchrotron GIXRD measurement. P3BT and P3HS homopolymers display (100) diffraction patterns along the out-of-plane (q_z) direction, which is indicative of an edge-on orientation with respect to the substrate (Figure S6). Their 1D GIXRD profiles show the (100) diffraction of P3BT and P3HS at the scattering vector (q_z) of 5.10 and 4.00 nm^{-1}, corresponding to the interlayer spacing (d_{100}) of 12.3 and 15.7 Å, respectively (Figure S6b and Table 3). The π-π stacking distance (d_{010}) of P3BT and P3HS is 3.75 and 3.89 Å, deriving from the scattering vector ($q_{x,y}$) along the in-plane direction at 16.75 and 16.14 nm^{-1}, respectively (Figure S6c and Table 3). The P3HS homopolymer shows a higher crystallinity revealed by stronger intensity of (100) diffraction peak. A further detailed analysis indicates that the P3HS homopolymer has a narrower full width at half maxima (FWHM) of (100) peak ($FWHM_{100,P3HS}$ = 0.435 nm^{-1}) than that of P3BT homopolymer ($FWHM_{100,P3BT}$ = 0.591 nm^{-1}) (Fig. 5). Since the narrower FWHM means the narrower distribution of chain conformations and more ordered structure [37,38],

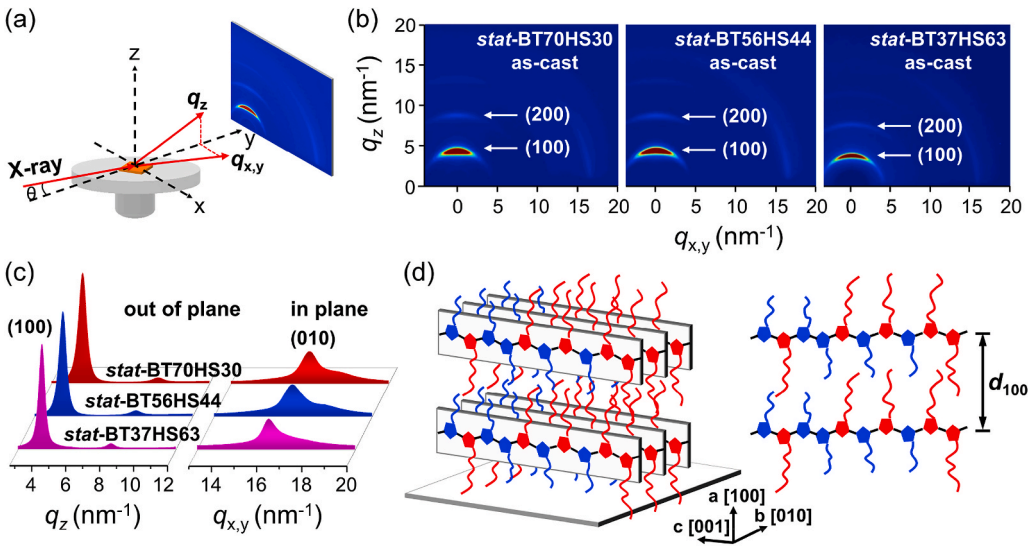

Fig. 4. (a) Schematic of 2D-GIXRD characterization for P3BT-*stat*-P3HS statistical copolymers with the incidence angle of the X-ray beam of 0.15°. q_z and $q_{x,y}$ are out-of-plane and in-plane direction, respectively. (b) 2D-GIXRD profiles from P3BT-*stat*-P3HS thin films with various molar ratios of thiophene to selenophene in as-cast state. (c) The corresponding 1D GIXRD profiles of three P3HT-*stat*-P3BS thin films. (d) Schematic of chain packing mode in P3BT-*stat*-P3HS crystals. The a-axis, b-axis, and c-axis represent the alkyl stacking direction, the π-π stacking direction, and the backbone direction, respectively.

Table 3
Summary of crystallographic parameters of P3BT-*stat*-P3HS statistical copolymers, P3BT and P3HS Homopolymers, and P3BT/P3HS blend.

polymers	as-cast				150 °C				$\triangle N_{100}$ [e]
	d_{100} (nm) [a]	L_{100} (nm) [b]	N_{100} [c]	d_{010} (nm) [d]	d_{100} (nm) [a]	L_{100} (nm) [b]	N_{100} [c]	d_{010} (nm) [d]	
P3BT	1.23	9.48	7.71	0.375	1.27	12.99	10.23	0.375	2.52
P3HS	1.57	12.87	8.20	0.389	1.58	21.29	13.48	0.388	5.28
P3BT/P3HS	1.25/1.57	–	–	0.376/0.388	1.30/1.58	–	–	0.375/0.388	-
stat-BT70HS30	1.39	10.09	7.26	0.380	1.41	13.46	9.55	0.378	2.29
stat-BT56HS44	1.44	11.09	7.70	0.381	1.46	15.09	10.34	0.380	2.64
stat-BT37HS63	1.53	12.93	8.45	0.387	1.52	17.83	11.73	0.387	3.28

[a] Lamellar distance.
[b] Coherence length through the lamellar direction.
[c] The number of lamellar packing layers, i.e., $N_{100} = L_{100}/d_{100}$.
[d] π-π stacking distance.
[e] The increment of lamellar packing layers, i.e., $\triangle N_{100} = N_{100,150\ °C} - N_{100,as\text{-}cast}$.

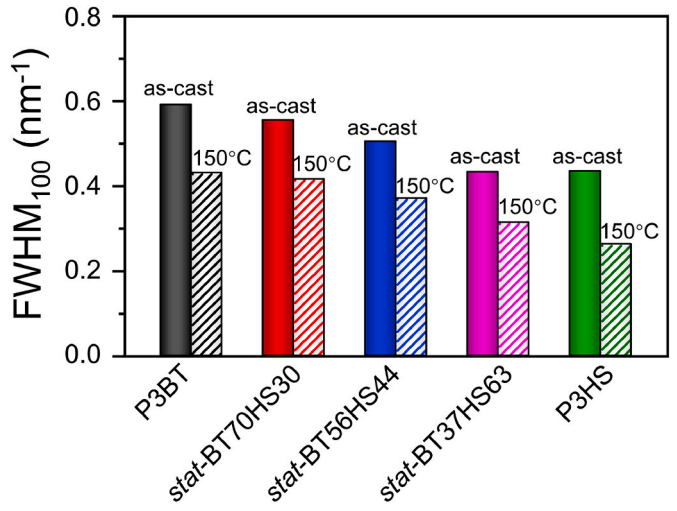

Fig. 5. The histograms summarizing the full width at half maximum (FWHM) of (100) diffraction peaks of P3BT-*stat*-P3HS thin films with various molar ratios of thiophene to selenophene and P3BT and P3HS at as-cast and 150°-annealed states.

it implies the P3HS displays more ordered crystalline structure in (100) direction than P3BT homopolymer. Because P3HS has a better solubility due to a longer alkyl side chains and higher planarity of backbone than P3BT, it may form a more ordered crystalline structure in (100) direction than P3BT.

For three thin films of P3BT-*stat*-P3HS, all copolymers exhibited only one (100) peak in the direction of out-of-plane, with q_z of 4.52 nm^{-1} (d_{100} = 13.9 Å) for *stat*-BT70HS30, 4.36 nm^{-1} (d_{100} = 14.4 Å) for *stat*-BT56HS44, and 4.10 nm^{-1} (d_{100} = 15.3 Å) for *stat*-BT37HS63, respectively (Fig. 4b-c and Table 3). The d_{010} values of three P3BT-*stat*-P3HS are 3.80, 3.81, and 3.87 Å for *stat*-BT70HS30, *stat*-BT56HS44, and *stat*-BT37HS63, with the $q_{x,y}$ at 16.53, 16.48, and 16.23 nm^{-1}, respectively (Table 3). Both d_{100} and d_{010} values of the statistical copolymers are between those of P3BT and P3HS homopolymers and increased gradually with the increased content of selenophene units, due to the fact that the hexyl chains on the selenophene rings are longer than the butyl chains on the thiophene rings and the Se atom is larger than the S atom as well. By comparison, with the increased content of selenophene units in the statistical copolymers, the FWHM of their (100) diffraction peak decreased (Fig. 5). The as-cast *stat*-BT37HS63 has the smallest FWHM$_{100}$ of 0.433 nm^{-1}. Since the FWHM reflects the crystallite size and disorder within the crystal, it suggests an increased ordering along the (100) direction in P3BT-*stat*-P3HS with the increased content of selenophene. These GIXRD data indicate that thiophene and selenophene chains in the copolymers form crystals in an edge-on configuration, confirming the semi-crystalline properties of all three statistical copolymers despite their random sequence architectures. In contrast, there were two (100) peaks at q_z of 4.01 (d_{100} = 15.7 Å) and 5.02 nm^{-1} (d_{100} = 12.5 Å) for the P3BT/P3HS blend at as-cast state, implying that P3BT and P3HS crystallized individually (Figure S6 and Table 3). Since P3BT and P3HS have

different crystallization kinetics, they crystallized separately to form respective crystalline domains in the blend during the solvent evaporation process. While the covalent bond between thiophene and selenophene units in the statistical copolymers help them to crystallize together. The schematic of the possible chain arrangement of P3BT-*stat*-P3HS crystals in an edge-on orientation is depicted in Fig. 4d. The randomly distributed butyl and hexyl side chains connected to the main backbone yield a uniform d_{100}-spacing in each statistical copolymer.

Thermal annealing has been widely utilized as an effective strategy to improve the degree of order of polymer chain stacking. In this study, three P3BT-*stat*-P3HS samples were undergone thermal treatment at 150 °C for 30 min and subsequently scrutinized by 2D-GIXRD (Fig. 6). Compared to as-cast samples, all three P3BT-*stat*-P3HS copolymers displayed one more intense and sharper (100) diffraction peaks, an indicative of the maintenance of their crystallization structures with increased crystallinity. Their crystallographic parameters including d_{100} and d_{010} remained or slightly changed after thermal annealing (Table 3). The corresponding FWHM of their (100) diffraction peaks is narrower after 150 °C thermal annealing, which is 0.416, 0.371, and 0.314 nm^{-1} for *stat*-BT70HS30, *stat*-BT56HS44, and *stat*-BT37HS63, respectively, indicative of a more ordered crystalline structure (Fig. 5). The reference samples of P3BT, P3HS and P3BT/P3HS blend showed increased crystallinity deduced from 2D-GIXRD Results (Figure S7). The FWHM of P3BT and P3HS (100) diffraction peaks become narrower after thermal annealing as well, which is 0.431 and 0.263 nm^{-1}, respectively (Fig. 5). It implies an improved ordering and the growth of crystallite size of the statistical copolymers and homopolymers after thermal annealing.

In order to further probe the crystallization behavior of the statistical copolymers, TGA and DSC measurements were carried out. The thermal properties of the statistical copolymers were first investigated to determine a proper upper limit temperature to avoid the thermal decomposition of the copolymers during the DSC tests. It shows all statistical copolymers exhibited excellent thermal stability and the 5% weight loss occurs at the temperature above 390 °C (i.e., 395 °C for *stat*-BT37HS63, 421 °C for *stat*-BT56HS44, and 436 °C for *stat*-BT70HS30, respectively) (Figure S8). The thermal decomposition temperature of these statistical copolymers decreased with the increased content of selenophene components, due to the higher thermal decomposition temperature of P3BT (486 °C) than that of P3HS (382 °C). As a result, the upper limit temperature for DSC is chosen to be 300 °C, below which all statistical copolymers and homopolymers are thermally stable. As shown in Fig. 7, for reference samples, the melting temperature (T_m) of P3BT and P3HS homopolymers was 286 and 214 °C, respectively. All three P3BT-*stat*-P3HS copolymers exhibited one evident endothermic peak, with their T_m at 203, 212 and 234 °C for *stat*-BT37HS63, *stat*-BT56HS44, and *stat*-BT70HS30, respectively. It further confirms their semicrystalline and crystalline nature. Their T_ms were closer to the T_m of P3HS homopolymer and were found to decrease with the increased content of selenophene component. Notably, the T_m of *stat*-BT37HS63 was even lower than that of P3HS homopolymer. The reduced regularity of the copolymer chains owing to the random distribution of the two monomer units along the backbone may account for it. Unlike statistical copolymers,

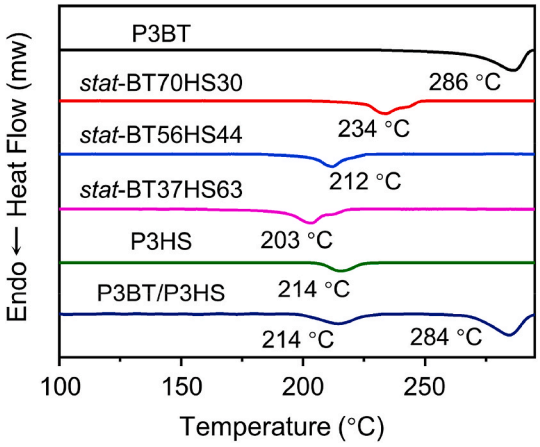

Fig. 7. DSC endotherms of three P3BT-*stat*-P3HS statistical copolymers, P3BT, P3HS, and the P3BT/P3HS blend.

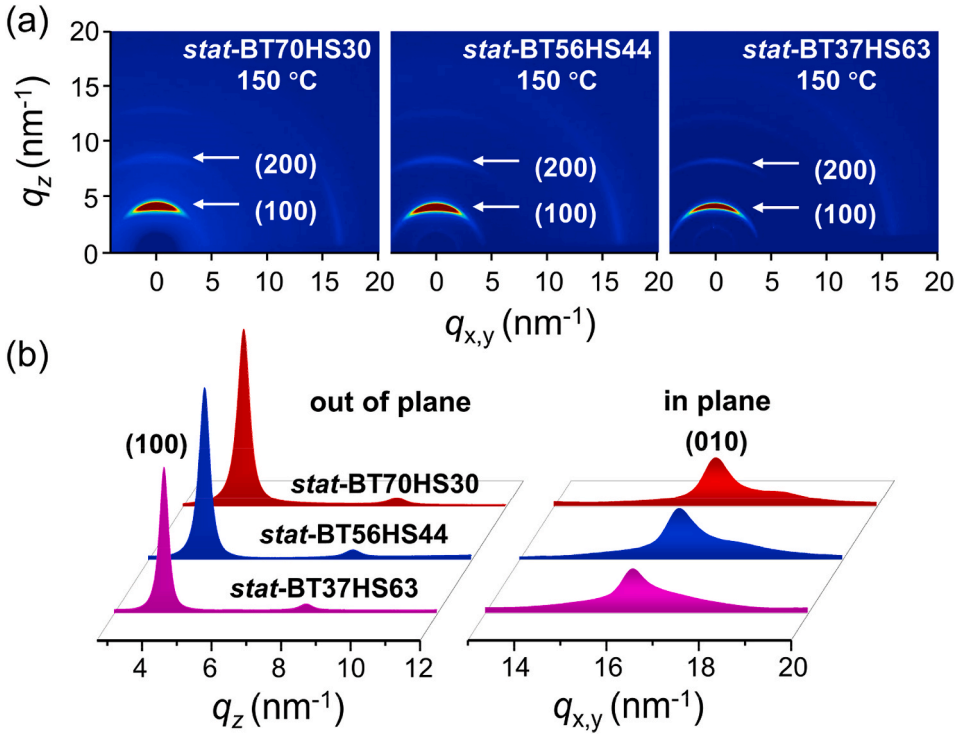

Figure 6. (a) 2D-GIXRD profiles and the resulting (b) 1D GIXRD images of three P3BT-*stat*-P3HS thin films after 150 °C-annealing.

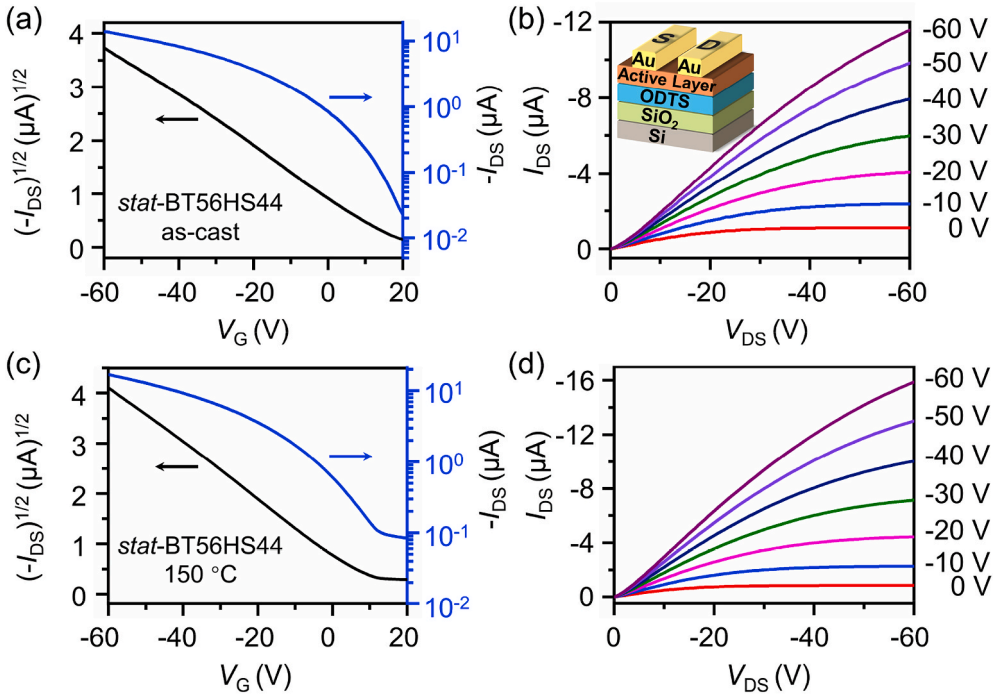

Fig. 8. (a, c) Transfer and (b, d) output curves of OFETs based on *stat*-BT56HS44 thin films in (a, b) as-cast and (c, d) 150 °C-annealed states. $V_{DS} = -60$ V. Inset in (b) is the schematic of OFET structure.

however, there are two separated endothermic peaks in the P3BT/P3HS blend, with 214 and 284 °C corresponding to P3HS and P3BT, respectively. It further proved respective crystal domains in the blend.

To evaluate the charge transport properties of P3BT-*stat*-P3HS statistical copolymers, bottom-gate top-contact OFET devices were crafted. Devices with P3BT, P3HS and P3BT/P3HS blend as active layers were fabricated under the same condition for comparison. The transfer and output curves of *stat*-BT56HS44 are shown in Fig. 8 as an example. These curves of other samples including *stat*-BT70HS30, *stat*-BT37HS63 as well as control samples including P3BT, P3HS, and P3BT/P3HS blend are given in Figures S9-S13. The OFET performances of three P3BT-*stat*-P3HS along with control samples are summarized in Table 4, with their charge mobilities comparable to the reported polythiophenes and polyselenophenes [39,40]. The as-cast statistical copolymers exhibited excellent device performance as to field-effect mobilities (5.9×10^{-2} cm^2 V^{-1} s^{-1} for *stat*-BT70HS30, 5.5×10^{-2} cm^2 V^{-1} s^{-1} for *stat*-BT56HS44, and 3.0×10^{-2} cm^2 V^{-1} s^{-1} for *stat*-BT37HS63) without any further thermal or solvent treatments (Fig. 8a-b, Figure S9-S10, and Table 4), higher than those of parent homopolymers as well as the corresponding blend (2.0×10^{-2} cm^2 V^{-1} s^{-1} for P3BT, 2.3×10^{-2} cm^2 V^{-1} s^{-1} for P3HS, and 1.0×10^{-2} cm^2 V^{-1} s^{-1} for P3BT/P3HS blend) (Figure S11-S13 and Table 4). It indicates excellent compatibility and synergy of thiophene and selenophene components connected through covalent bond within the mainchains. Since the thiophene units packed more closely, which favors interchain charge transport, and the selenophene units of higher planarity facilitates intrachain charge transport, the crystals formed in P3BT-*stat*-P3HS copolymers possess the synergy of two conjuaged units which facilitates the charge transport. On the contrary, the P3BT/P3HS blend showed lower charge mobility than P3BT-*stat*-P3HS crystals and its parent homopolymers. As mentioned before, the P3BT and P3HS tended to crystalize individually in the blend, leading to a great number of grain boundaries as well as shortage of bridging chains between crystalline domains. Hence, it is not surprising that the performance of the P3BT/P3HS-based OFET is inferior to both statistical copolymers and P3BT and P3HS homopolymers.

A further in-depth analysis indicates aside from P3BT, the mobility of

Table 4
Summary of OFET performances of P3BT-*stat*-P3HS statistical copolymers, P3BT and P3HS homopolymers, and P3BT/P3HS blend.

Polymers	Conditions	μ_{max} [a] (cm^2 V^{-1} s^{-1})	μ_{avg} [b] (cm^2 V^{-1} s^{-1})	I_{on}/I_{off} [c]	V_{th} [d] (V)
P3BT	as-cast	2.1×10^{-2}	2.0×10^{-2}	10^3–10^6	7–17
	150 °C	2.4×10^{-2}	2.2×10^{-2}	10^3–10^5	5–13
P3HS	as-cast	2.5×10^{-2}	2.3×10^{-2}	10^3–10^6	−3–2
	150 °C	3.1×10^{-2}	2.8×10^{-2}	10^3–10^7	−2–4
P3BT/P3HS	as-cast	1.2×10^{-2}	1.0×10^{-2}	10^2–10^5	13–24
	150 °C	1.9×10^{-2}	1.5×10^{-2}	10^2–10^5	6–23
stat-BT70HS30	as-cast	6.7×10^{-2}	5.9×10^{-2}	10^2–10^4	6–12
	150 °C	7.2×10^{-2}	6.8×10^{-2}	10^3–10^5	7–15
stat-BT56HS44	as-cast	6.0×10^{-2}	5.5×10^{-2}	10^3–10^4	8–13
	150 °C	6.7×10^{-2}	6.1×10^{-2}	10^3–10^5	8–18
stat-BT37HS63	as-cast	3.5×10^{-2}	3.0×10^{-2}	10^2–10^4	−1–8
	150 °C	4.9×10^{-2}	4.3×10^{-2}	10^3–10^5	6–10

[a] Maximum charge carrier mobility.
[b] Average charge carrier by measuring at least 12 OFET devices.
[c] Current on/off ratio.
[d] Threshold voltage.

three P3BT-*stat*-P3HS statistical copolymers and P3HS homopolymer with different selenophene content were in reverse proportion to their π-π stacking distance d_{010} (Fig. 9). With the increased selenophene content, the d_{010} of *stat*-BT70HS30, *stat*-BT56HS44, *stat*-BT37HS63, and P3HS gradually increased from 3.80, 3.81, 3.87, to 3.89 Å, respectively. Instead, their mobility decreased from 5.9 × 10^{-2}, 5.5 × 10^{-2}, 3.0 × 10^{-2}, to 2.3 × 10^{-2} $cm^2 V^{-1} s^{-1}$. A plausible explanation on the reverse variation trend in mobility of samples with the increasing selenophene content as well as the increasing d_{010} may be as follows. The mobility of P3BT is relatively low due to its poor solubility resulted from high molecular weight as well as short alkyl side chains. When statistically introducing selenophene units into the backbone of P3BT, on one hand, it endows P3BT with good solubility and improves the coplanarity of the heterocycles within the backbone, which are beneficial to charge travel. On the other hand, it inevitably increases the π-π stacking distance. Since the direction of π−π stacking is one of the efficient directions for charge carriers to travel, the increased d_{010} is unfavorable for the charge transport. Accordingly, the actual charge mobility depends on which effect dominates. When incorporating a small amount of selenophene constituents, the *stat*-BT70HS30 has enhanced solubility, more planar backbone, along with moderate d_{010}. All these factors made it has the highest mobility among all investigated systems. Continuously increasing the selenophene content led to the d_{010}-factor dominated, resulting in the decreased charge mobilities in *stat*-BT56HS44, *stat*-BT37HS63, and P3HS.

After 150 °C thermal annealing, all statistical copolymers demonstrated slightly higher charge mobilities, i.e., 6.8 × 10^{-2}, 6.1 × 10^{-2}, and 4.3 × 10^{-2} $cm^2 V^{-1} s^{-1}$ for *stat*-BT70HS30, *stat*-BT56HS44, and *stat*-BT37HS63, respectively, than those in as-cast state (Fig. 8c-d, Figure S9-S10, and Table 4). Similarly, the reference samples displayed increased charge mobilities as well, which are 2.2 × 10^{-2} $cm^2 V^{-1} s^{-1}$ for P3BT, 2.8 × 10^{-2} $cm^2 V^{-1} s^{-1}$ for P3HS, and 1.5 × 10^{-2} $cm^2 V^{-1} s^{-1}$ for P3BT/P3HS blend, respectively (Figure S11-S13 and Table 4). The slightly increased charge mobilities for all samples is not surprising as these samples showed higher crystallinities as well as more ordered crystalline structures after being thermally treated, reflected by GIXRD Results. A further detailed investigation into their crystalline structure was carried out by calculating the structural coherence length through the (100) direction (L_{100}) before and after thermal annealing. The coherence length can be quantified via the Scherrer equation $L = K\lambda/B\cos\theta$, where L is the crystallite size, K is a dimensionless crystallite-shape factor, λ is the X-ray wavelength, θ is the Bragg angle, and B is the FWHM of the X-ray diffraction peak [41,42]. The Scherrer equation is commonly used to estimate the crystallite size which is based on the assumptions that its size is the main factor to broad the diffraction peaks and the disorder of lattice can be ignored [37]. As shown in Table 3, *stat*-BT70HS30, *stat*-BT56HS44, and *stat*-BT37HS63 show the L_{100} of 10.09, 11.09, and 12.93 nm, and they all increased to 13.46, 15.09, and 17.83 nm, respectively, after thermal annealing. By calculating the number of alkyl stacking layers (N_{100}) from the ratio of L_{100}/d_{100} ($N_{100} = L_{100}/d_{100}$), *stat*-BT70HS30, *stat*-BT56HS44, and *stat*-BT37HS63 display the N_{100} of 7.26, 7.70, and 8.45, respectively, at as-cast state. After 150 °C-annealing, they all increased to 9.55, 10.34, and 11.73, with the increment ($\triangle N_{100}$) of 2.29, 2.64, and 3.28, respectively. The increased L_{100} and N_{100} of three P3BT-*stat*-P3HS statistical copolymers indicate their increased crystalline size and improved ordering along the (100) direction. Similar trend of increased L_{100} and N_{100} after 150 °C-annealing was observed in P3BT and P3HS homopolmers (Table 3). In light of the increased order and crystallite size through the (100) direction, it is reasonable that these P3BT-*stat*-P3HS and the corresponding homopolymers display enhanced charge mobilities after thermal annealing.

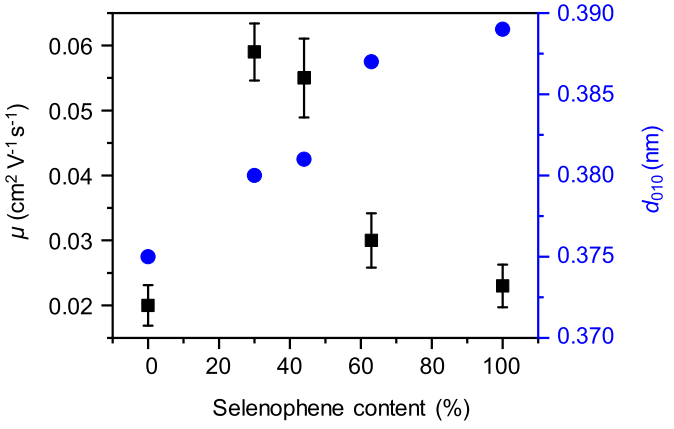

Fig. 9. Plot of field-effect mobility and d_{010} as a function of selenophene content.

To further elucidate the film microstructure and quality, all P3BT-*stat*-P3HT thin films in as-cast state and after 150 °C thermal annealing were probed by AFM (Figure S14). It shows that the morphology of all P3BT-*stat*-P3HS thin films were featureless and their film surfaces were relatively smooth with the root-mean-square roughness of 4.37 nm, 2.18 nm, and 1.35 nm in *stat*-BT70HS30, *stat*-BT56HS44 and *stat*-BT37HS63, respectively. The statistical copolymer with a higher content of selenophene unit has a smaller root-mean-square roughness. After 150 °C thermal annealing, their root-mean-square roughness decreased slightly (i.e., 4.19 nm, 1.91 nm, and 1.05 nm for *stat*-BT70HS30, *stat*-BT56HS44 and *stat*-BT37HS63, respectively), indicating that thermal annealing yielded a smoother surface for more efficient charge transport in each P3BT-*stat*-P3HS thin film.

4. Conclusions

In summary, we have judiciously designed and synthesized a set of P3BT-*stat*-P3HS statistical copolymers with tunable molar ratios of thiophene to selenophene via GRIM polymerization. The bandgap of the materials could be finely tuned by simply varying the ratio of thiophene to selenophene. By means of 2D-GIXRD together with DSC, the crystalline nature and the edge-on orientation of the statistical copolymers were confirmed regardless of the random sequence architectures, which were favourable and crucial to high charge mobilities. Intriguingly, the three P3BT-*stat*-P3HS statistical copolymers exhibited excellent field-effect mobilities without any further thermal or solvent treatments, exceeding P3BT and P3HS homopolymers and P3BT/P3HS blend, with the average charge mobility of *stat*-BT70HS30 reaching as high as 0.059 $cm^2V^{-1}s^{-1}$. Since the thiophene and selenophene units were covalently connected in P3BT-*stat*-P3HS copolymers, their crystals possess the synergy of two conjuaged components since the P3BT chains packed more closely which favored the interchain charge transport and the P3HS chains of higher planarity facilitated intrachain charge transport. Further enhancement of charge mobility can be expected by subtly tuning the selenophene content in P3BT-*stat*-P3HS statistical copolymers. On the contrary, the P3BT/P3HS blend displayed lower charge mobility than P3BT-*stat*-P3HS crystals and its parent homopolymers. Due to the difference in crystallization kinetics, P3BT and P3HS in the blend crystallized individually which led to separated domains and numerous grain boundaries without sufficient bridging chains, contributing to the relatively low mobility eventually. It highlights the advantages of statistical copolymers over conventional blends in this system. After 150 °C thermal annealing, all P3BT-*stat*-P3HS statistical copolymers exhibited slightly higher charge mobilities in comparison with those in as-cast state, due to the improvement in crystallinities. Overall, such advantages as tunable bandgap, crystalline nature and relatively high mobilities in P3BT-*stat*-P3HS statistical copolymers make them become promising candidates for applications in a wide range of optoelectronic devices.

Declaration of competing interest

The authors declare no competing financial interests.

Acknowledgements

This work is supported by the National Natural Science Foundation of China (21922503). We gratefully acknowledge the support from Shanghai Synchrotron Radiation Facility of China for using the BL14B1 and BL16B1 beamlines.

Appendix A. Supplementary data

Supplementary data to this article can be found online at https://doi.org/10.1016/j.polymer.2021.123854.

References

[1] J. Xu, H.C. Wu, C. Zhu, A. Ehrlich, L. Shaw, M. Nikolka, S. Wang, F. Molina-Lopez, X. Gu, S. Luo, D. Zhou, Y.H. Kim, G.N. Wang, K. Gu, V.R. Feig, S. Chen, Y. Kim, T. Katsumata, Y.Q. Zheng, H. Yan, J.W. Chung, J. Lopez, B. Murmann, Z. Bao, Multi-scale ordering in highly stretchable polymer semiconducting films, Nat. Mater. 18 (2019) 594–601.
[2] Z.F. Yao, Z.Y. Wang, H.T. Wu, Y. Lu, Q.Y. Li, L. Zou, J.Y. Wang, J. Pei, Ordered solid-state microstructures of conjugated polymers arising from solution-state aggregation, Angew. Chem. Int. Ed. 59 (2020) 17467–17471.
[3] K. Gu, Y.L. Loo, The polymer physics of multiscale charge transport in conjugated systems, J. Polym. Sci., Part B: Polym. Phys. 57 (2019) 1559–1571.
[4] P.M. Beaujuge, J.M. Frechet, Molecular design and ordering effects in π-functional materials for transistor and solar cell applications, J. Am. Chem. Soc. 133 (2011) 20009–20029.
[5] L. Zhou, L. Shen, J. Huang, N. Liu, Y.Y. Zhu, Z.Q. Wu, Optically active helical polyisocyanides bearing chiral phosphine pendants: facile synthesis and application in enantioselective Rauhut-Currier reaction, Chin. J. Polym. Sci. 36 (2018) 163–170.
[6] L. Xu, C. Wang, Y.X. Li, X.H. Xu, L. Zhou, N. Liu, Z.Q. Wu, Crystallization-driven asymmetric helical assembly of conjugated block copolymer and the aggregation induced white-light emission and circularly polarized luminescence, Angew. Chem. Int. Ed. 59 (2020) 16675–16682.
[7] L. Xu, X.H. Xu, N. Liu, H. Zou, Z.Q. Wu, A facile synthetic route to multifunctional poly(3-hexylthiophene)-*b*-poly(phenyl isocyanide) copolymers: from aggregation-induced emission to controlled helicity, Macromolecules 51 (2018) 7546–7555.
[8] K.S. Park, J.J. Kwok, P. Kafle, Y. Diao, When assembly meets processing: tuning multiscale morphology of printed conjugated polymers for controlled charge transport, Chem. Mater. 33 (2021) 469–498.
[9] D. Tao, C. Feng, Y. Cui, X. Yang, I. Manners, M.A. Winnik, X. Huang, Monodisperse fiber-like micelles of controlled length and composition with an oligo(p-phenylenevinylene) core via "living" crystallization-driven self-assembly, J. Am. Chem. Soc. 139 (2017) 7136–7139.
[10] D. Tao, C. Feng, Y. Lu, Y. Cui, X. Yang, I. Manners, M.A. Winnik, X. Huang, Self-seeding of block copolymers with a π-conjugated oligo(p-phenylenevinylene) segment: a versatile route toward monodisperse fiber-like nanostructures, Macromolecules 51 (2018) 2065–2075.
[11] D. Tao, Z. Wang, X. Huang, M. Tian, G. Lu, I. Manners, M.A. Winnik, C. Feng, Continuous and segmented semiconducting fiber-like nanostructures with spatially selective functionalization by living crystallization-driven self-assembly, Angew. Chem. Int. Ed. 59 (2020) 8232–8239.
[12] H. Yang, R. Zhang, L. Wang, J. Zhang, X. Yu, Y. Geng, Y. Han, Crystallization assisted microphase separation in all-conjugated phenylene-thiophene diblock copolymers, Polymer 97 (2016) 238–246.
[13] L. Xu, J. Zhang, J. Peng, F. Qiu, Formation of nanofibers in poly(9,9-dioctylfluorene) toluene solutions during aging, J. Polym. Sci., Part B: Polym. Phys. 53 (2015) 633–639.
[14] S. Pan, M. Zhu, L. He, H. Zhang, F. Qiu, Z. Lin, J. Peng, Transformation from nanofibers to nanoribbons in poly(3-hexylthiophene) solution by adding alkylthiols, Macromol. Rapid Commun. 39 (2018), 1800048.
[15] Y.-H. Lee, W.-C. Yen, W.-F. Su, C.-A. Dai, Self-assembly and phase transformations of p-conjugated block copolymers that bend and twist: from rigid-rod nanowires to highly curvaceous gyroids, Soft Matter 7 (2011) 10429–10442.
[16] G.H. Lu, L.G. Li, X.N. Yang, Achieving perpendicular alignment of rigid polythiophene backbones to the substrate by using solvent-vapor treatment, Adv. Mater 19 (2007) 3594–3598.
[17] D. Miyajima, F. Araoka, H. Takezoe, J. Kim, K. Kato, M. Takata, T. Aida, Electric-field-responsive handle for large-area orientation of discotic liquid-crystalline molecules in millimeter-thick Films, Angew. Chem. Int. Ed. 50 (2011) 7865–7869.
[18] M. Zhu, S. Pan, Y. Wang, P. Tang, F. Qiu, Z. Lin, J. Peng, Unravelling the correlation between charge mobility and cocrystallization in rod–rod block copolymers for high-performance field-effect transistors, Angew. Chem. Int. Ed. 57 (2018) 8644–8648.
[19] S. Agbolaghi, S. Zenoozi, A comprehensive review on poly (3-alkylthiophene)-based crystalline structures, protocols and electronic applications, Org, Electron 51 (2017) 362–403.
[20] A. Patra, M. Bendikov, Polyselenophenes, J. Mater. Chem. 20 (2010) 422–433.
[21] H.J. Yun, J. Cho, D.S. Chung, Y.H. Kim, S.K. Kwon, Comparative studies on the relations between composition ratio and charge transport of diketopyrrolopyrrole-based random copolymers, Macromolecules 47 (2014) 7030–7035.
[22] C.H. Tsai, A. Fortney, Y. Qiu, R.R. Gil, D. Yaron, T. Kowalewski, K.J.T. Noonan, Conjugated polymers with repeated sequences of group 16 heterocycles synthesized through catalyst-transfer polycondensation, J. Am. Chem. Soc. 138 (2016) 6798–6804.
[23] N.K. Obhi, D.M. Peda, E.L. Kynaston, D.S. Seferos, Exploring the graft-to synthesis of all-conjugated comb copolymers using azide–alkyne click chemistry, Macromolecules 51 (2018) 2969–2978.
[24] Y.-Y. Lai, T.-C. Tung, W.-W. Liang, Y.-J. Cheng, Synthesis of poly(3-hexylthiophene), poly(3-hexylselenophene), and poly(3-hexylselenophene-alt-3-hexylthiophene) by direct C−H arylation polymerization via N-heterocyclic carbene palladium catalysts, Macromolecules 48 (2015) 2978–2988.
[25] Y.H. Lee, W.C. Chen, Y.L. Yang, C.J. Chiang, T. Yokozawa, C.A. Dai, Co-crystallization phase transformations in all pi-conjugated block copolymers with different main-chain moieties, Nanoscale 6 (2014) 5208–5216.
[26] P. Wu, G. Ren, S.A. Jenekhe, Crystalline random conjugated copolymers with multiple side chains: tunable intermolecular interactions and enhanced charge transport and photovoltaic properties, Macromolecules 43 (2010) 3306–3313.
[27] E.F. Palermo, A.J. McNeil, Impact of copolymer sequence on solid-state properties for random, gradient and block copolymers containing thiophene and selenophene, Macromolecules 45 (2012) 5948–5955.
[28] J.H. Bannock, M. Al-Hashimi, S.H. Krishnadasan, J.J.M. Halls, M. Heeney, J.C. de Mello, Controlled synthesis of conjugated random copolymers in a droplet-based microreactor, Mater. Horiz 1 (2014) 214–218.
[29] H. Yan, J. Hollinger, C.R. Bridges, G.R. McKeown, T. Al-Faouri, D.S. Seferos, Doping poly(3-hexylthiophene) nanowires with selenophene increases the performance of polymer-nanowire solar cells, Chem. Mater. 26 (2014) 4605–4611.
[30] A. Fortney, C.-H. Tsai, M. Banerjee, D. Yaron, T. Kowalewski, K.J.T. Noonan, Impact of precise control over microstructure in thiophene−selenophene copolymers, Macromolecules 51 (2018) 9494–9501.
[31] A. Yokoyama, R. Miyakoshi, T. Yokozawa, Chain-growth polymerization for poly (3-hexylthiophene) with a defined molecular weight and a low polydispersity, Macromolecules 37 (2004) 1169–1171.
[32] S. Chen, L. Li, D. Zhai, Y. Yin, X. Shang, B. Ni, J. Peng, Cocrystallization-promoted charge mobility in all-conjugated diblock copolymers for high-performance field-effect transistors, ACS Appl. Mater. Interfaces 12 (2020) 58094–58104.
[33] D. Braga, G. Horowitz, High-performance organic field-effect transistors, Adv. Mater 21 (2009) 1473–1486.
[34] M.J. Frisch, G.W. Trucks, H.B. Schlegel, G.E. Scuseria, M.A. Robb, J.R. Cheeseman, J.A. Montgomery Jr., T. Vreven, K.N. Kudin, J.C. Burant, J.M. Millam, S.S. Iyengar, J. Tomasi, V. Barone, B. Mennucci, M. Cossi, G. Scalmani, N. Rega, G.A. Petersson, H. Nakatsuji, M. Hada, M. Ehara, K. Toyota, R. Fukuda, J. Hasegawa, M. Ishida, T. Nakajima, Y. Honda, O. Kitao, H. Nakai, M. Klene, X. Li, J.E. Knox, H. P. Hratchian, J.B. Cross, V. Bakken, C. Adamo, J. Jaramillo, R. Gomperts, R. E. Stratmann, O. Yazyev, A.J. Austin, R. Cammi, C. Pomelli, J.W. Ochterski, P. Y. Ayala, K. Morokuma, G.A. Voth, P. Salvador, J.J. Dannenberg, V.G. Zakrzewski, S. Dapprich, A.D. Daniels, M.C. Strain, O. Farkas, D.K. Malick, A.D. Rabuck, K. Raghavachari, J.B. Foresman, J.V. Ortiz, Q. Cui, A.G. Baboul, S. Clifford, J. Cioslowski, B.B. Stefanov, G. Liu, A. Liashenko, P. Piskorz, I. Komaromi, R. L. Martin, D.J. Fox, T. Keith, M.A. Al-Laham, C.Y. Peng, A. Nanayakkara, M. Challacombe, P.M.W. Gill, B. Johnson, W. Chen, M.W. Wong, C. Gonzalez, J. A. Pople, Gaussian, Inc., 2004. Wallingford CT.
[35] N. Berube, V. Gosselin, J. Gaudreau, M. Cote, Designing polymers for photovoltaic applications using ab initio calculations, J. Phys. Chem. C 117 (2013) 7964–7972.
[36] Y.K. Lan, C.I. Huang, Charge mobility and transport behavior in the ordered and disordered states of the regioregular poly (3-hexylthiophene), J. Phys. Chem. B 113 (2009) 14555–14564.
[37] J. Rivnay, R. Noriega, R.J. Kline, A. Salleo, M.F. Toney, Quantitative analysis of lattice disorder and crystallite size in organic semiconductor thin films, Phys. Rev. B 84 (2011), 045203.
[38] M. Park, A. Aiyar, J. Park, E. Reichmanis, M. Srinivasarao, Solvent evaporation induced liquid crystalline phase in poly (3-hexylthiophene), J. Am. Chem. Soc. 133 (2011) 7244–7247.
[39] Y. Wang, H. Cui, M. Zhu, F. Qiu, J. Peng, Z. Lin, Tailoring phase transition in poly (3-hexylselenophene) thin films and correlating their crystalline polymorphs with charge transport properties for organic field-effect transistors, Macromolecules 50 (2017) 9674–9682.
[40] X. Shang, Y. Yin, S. Chen, M. Zhu, D. Zhai, X. Liu, J. Peng, Unravelling the correlation between microphase separation and cocrystallization in thiophene-selenophene block copolymers for organic field-effect transistors, Macromolecules 53 (2020) 10245–10255.
[41] U. Holzwarth, N. Gibson, The Scherrer equation versus the 'Debye-Scherrer equation, Nat. Nanotechnol. 6 (2011), 534–534.
[42] K.A. Mazzio, A.H. Rice, M.M. Durban, C.K. Luscombe, Effect of regioregularity on charge transport and structural and excitonic coherence in poly (3-hexylthiophene) nanowires, J. Phys. Chem. C 119 (2015) 14911–14918.